FIELD PERTURBATIONS IN THE POST COUPLED DRIFT TUBE LINAC*

E. J. Schneider and D. A. Swenson
University of California, Los Alamos Scientific Laboratory
Los Alamos, New Mexico

Introduction

Several resonant coupling schemes have been proposed for the drift tube linac structure which produce vast improvements in the stability of the fields within the structure against perturbations such as mechanical detuning and beam loading. The resonant couplers can assume any of several forms but the ultimate in simplicity seems to be a post, mounted normal to the outer wall of the accelerator directly opposite the drift tubes and alternating from side to side of the cavity, as shown in Fig. 1.

The post couplers enjoy several advantages over other configurations of resonant couplers: The power dissipation on the post couplers can be quite small, they are readily tunable and have no mechanical interaction or electrical connection to the drift tube, they can be inserted through relatively small holes in the accelerator wall, and they allow access to the interior of the linac without disturbing the coupling mechanisms.

The resonantly-coupled linac structure is operated in the so-called $\pi/2$ mode, which has the property that the post couplers are unexcited in the lossless case with no tuning errors. In this idealized situation, the perturbations to the accelerating field due to the unexcited post couplers are quite small, as a result of their small size and favorable orientation.

In the practical case with losses and tuning errors, the post couplers are expected to have some small excitations. It has been suggested that the fields associated with these excited post couplers might have a detrimental effect on the dynamics of the particles traversing the structure.

A considerable effort has been made to measure the fields associated with the excited post couplers in the 35-cell model shown in Figs. 1 and 2. An indication of the relative excitation of the post couplers can be deduced from measurements of the magnetic field along the wall of the structure. These fields were measured by observing perturbations on the resonant frequency of the structure as a metallic slug was pulled along the outer wall. These data reveal the way in which the post coupler excitations depend on tuning errors and losses, and are in complete agreement with the predictions of the coupled resonator analysis.

Such evidence of post coupler excitation is not sufficient, however, to evaluate the effect of these excitations on the dynamics of the particles traversing the structure. For this purpose, it is necessary to search for perturbations to the normal accelerating fields near the axis of the linac produced by the excited post couplers. It has been

possible to detect some transverse fields on the axis of the linac by observing perturbations on the resonant frequency of the structure as a transverse metallic needle is rotated about the axis of the linac.

Assuming these fields to be proportional to the post coupler excitations, and making reasonable estimates of the post coupler excitations in an actual linac, the magnitudes of the transverse fields are found to be far below the value at which they would adversely affect the particle dynamics in the structure.

Coupled Resonator Analysis

Before describing the measurements and their analyses in detail, it is useful to present a few results of the coupled resonator analysis. The coupled resonator analysis has proven to be a valuable tool for explaining, understanding, and predicting the behavior of resonantly coupled accelerator structures in terms of the properties of simply and doubly periodic chains of coupled resonators.

The post coupled drift tube linac is usually described in terms of a biperiodic chain of coupled resonators with nearest and next nearest neighbor couplings operating in the $\pi/2$ cavity mode.[1-5] The structure is considered to be a chain of $2N + 1$ coupled resonators numbered from 0 to $2N$, where the even numbered resonators correspond to the accelerating cells and the odd numbered resonators correspond to the resonant post couplers.

Some very important properties of the structure are revealed, however, by investigating the $\pi/2$ mode of a uniform chain (not biperiodic) of $2N + 1$ coupled resonators with couplings between nearest neighbors only. The behavior of this chain may be represented by a system of equations of the form

$$I_n = X_n \left(1 + \frac{\omega_0}{j\omega Q_n} - \frac{\omega_0^2}{\omega^2}\right) + \frac{k}{2}\left(X_{n-1} + X_{n+1}\right)$$

where I_n is the drive, X_n is the field amplitude and Q_n is the quality factor in the nth resonator, ω_0 is the resonant frequency of the resonators in absence of coupling to the system, ω is the operating frequency, and k is the coupling factor between adjacent resonators.

Consider the case where $I_n = 0$, ω of the $\pi/2$ mode is ω_0, and ω_0 in the equation above is replaced by $\omega_0 + \Delta\omega_{0n}$, where $\Delta\omega_{0n}$ is the tuning error in the nth resonator. The coupled resonator equation for the $\pi/2$ mode becomes

$$\left(\Delta_n + \frac{2j}{kQ_n}\right) X_n = X_{n-1} + X_{n+1}$$

where

$$\Delta_n = \frac{4\Delta\omega_{0n}}{k\omega_0}, \text{ and terms in } \Delta\omega_{0n}^2 \text{ and } \Delta\omega_{0n}/Q_n$$

have been dropped.

The excitation of all resonators may be found in terms of the excitation of the end resonator X_0. Let $n = 0$ in the coupled resonator equation, and the equation becomes

$$\left(\Delta_0 + \frac{2j}{kQ_0}\right) X_0 = X_{-1} + X_1.$$

If we take the end cell to be a half cell terminated in a conducting sheet through the center of the cavity, X_{-1} will be the image of X_1 and the equation can be written

$$X_1 = \left(\frac{\Delta_0}{2} + \frac{j}{kQ_0}\right) X_0.$$

Let $n = 1$ in the coupled resonator equation, and the equation becomes

$$X_2 = \left(\Delta_1 + \frac{2j}{kQ_1}\right) X_1 - X_0$$

or

$$X_2 = -X_0 \left(1 + \frac{2}{k^2 Q_0 Q_1} + \text{terms in } \Delta_0 \Delta_1 \text{ and } \frac{j\Delta}{kQ}\right).$$

By continuing this process, we find that we can write general expressions for the excitation of all resonators.[6] For the odd resonators (post couplers), we get

$$X_{2n+1} = (-1)^n X_0 \left[\frac{-\Delta_0}{2} + \Delta_2 \right.$$

$$+ \ldots + \Delta_{2n} + \frac{j(2n+1)}{kQ_a} \left.\right], \qquad (1)$$

and for the even resonators (accelerating cells), we get

$$X_{2n} = (-1)^n X_0 \left[1 + n^2 \frac{2}{k^2 Q_a Q_c}\right.$$

$$+ \text{terms in } \Delta_a \Delta_c \text{ and } \frac{j\Delta}{kQ} \left.\right] \qquad (2)$$

These general equations reveal several interesting features of the $\pi/2$ mode. Equation 1 shows that the post excitations are proportional to the sum of the accelerating cell tuning errors between the end of the structure and the post in question. Measurements of post excitations presented in the next section are seen to be in agreement with this result. Equation 2 shows that the accelerating cell excitations are independent of tuning errors in both even and odd cells. This is simply a statement of the field stability properties of the

structure that we have described in previous reports.[2,3]

Relative Excitations of the Post Couplers

Post coupler excitations produce detectable magnetic fields along the outer wall of the structure. These fields, of course, are superimposed on the transverse magnetic field of the operating mode. The familiar perturbation technique offers a convenient means for measuring these magnetic fields, from which relative post excitations can be deduced. The technique consists of recording small variations in the resonant frequency of the structure as a metallic slug is pulled along the outer wall. The slug is offset to one side of the tank so as to be near the even numbered post as shown in Fig. 3. The slug affects the resonant frequency of the tank in such a way that the resonant frequency is high when the slug is in a region of high magnetic field, and low when the slug is in a region of low magnetic field.

Figures 4 and 5 are examples of the data collected by this technique. These measurements were made in our 35-cell model, where the geometry varies smoothly from 40 MeV at one end to 100 MeV at the other end. Figure 4a shows the normal variations of magnetic field on the wall of the structure with no post excitations. The magnetic field passes through a local maximum opposite each drift tube and a local minimum opposite each gap. The MESSYMESH field calculations tell us this variation should be about 2% at 40 MeV and 10% at 100 MeV. This explains why the variations are larger on the right hand end of these graphs.

Figures 4b and 4c show how these fields appear when the posts are strongly excited. The post excitations that contributed to Fig. 4b were produced by lowering the resonant frequency of cell 1 by 5 MHz, and raising the resonant frequency of cell 35 by about the same amount. In the case of Fig. 4c, the post excitations were produced by tuning errors of about the same magnitude but of the opposite sign. Equation 1 suggests that these error distributions should cause uniform excitation of all the posts in the tank.

Figure 6 shows a superposition of the transverse magnetic field of the operating mode and the magnetic fields of the post couplers. With the aid of this figure, it is quite easy to understand the data shown on Fig. 4b. Since the slug travels near the even numbered posts and far from the odd numbered posts, the magnetic fields are higher near the even numbered posts than near the odd numbered posts. Now consider the fields opposite gaps 31 and 32. The field from post 30 strengthens the field opposite gap 31, while the field from post 32 weakens the field opposite gap 32.

Reversing the sign of the tuning errors, as we did for Fig. 4c, reverses the sense of the post excitations. By reversing the sense of the post excitations on Fig. 6, it is easy to understand the data shown on Fig. 4c.

Figure 5a shows the field pattern recorded when tuning errors were introduced in cells 1 and 22. The resonant frequency of cell 1 was raised 3.5 MHz while the resonant frequency of cell 22 was lowered 3.5 MHz. Equation 1 suggests that all posts from 1 to 21 should be equally excited in the same sense as in Fig. 4c, and that all posts from 22 to 34 should be unexcited. Figure 5a readily verifies this prediction.

The field pattern in Fig. 5b was obtained by lowering the resonant frequency of cell 22 by 3.5 MHz and raising the resonant frequency of cell 35 by the same amount. Here Equation 1 suggests that all posts from 1 to 21 should be unexcited, and all posts from 22 to 34 should be equally excited in the same sense as in Fig. 4b. Here again, the prediction of the coupled resonator analysis is readily verified by inspection of Fig. 5b.

The importance of these measurements is to establish that the post excitations do depend on tuning errors as predicted by the coupled resonator analysis, and that even for crude alignment (Fig. 4a), the post excitations are unobservable.

The effect of power flow on post excitations was investigated briefly by this technique. If power flow excitations were observable, the magnetic field pattern along the wall would depend on the direction of power flow in the cavity and hence the position of the drive loop. Measurements were made with the drive loop in different locations and no differences were detected in the field pattern along the wall.

Transverse Needle Measurement Technique

The technique described below was developed in the hopes that it would provide a means for measuring small transverse electric fields on the axis of the linac in the presence of large axial accelerating fields. This technique like the previous one is based on the perturbation technique. For this measurement, small variations in the resonant frequency of the structure are recorded as a transverse metallic needle is rotated about the axis of the linac.

If the electric field in the gap has a transverse component, the resonant frequency of the structure should go through a minimum when the needle is aligned with the transverse component. This, of course, should happen twice for each needle rotation. In fact, if the needle is symmetric about its axis of rotation, the frequency perturbation should go through two identical excursions for each needle revolution (i.e., no first harmonic, mostly second harmonic). Almost all of our data shows some first harmonic, which we attribute to the fact that the needle is not exactly perpendicular to its axis of rotation.

The following simple analysis will help in the interpretation of the data presented in the next section. The frequency perturbation is proportional to the square of the component of the field in the direction of the needle. Let F be the field vector at the needle having a magnitude F in the direction of the unit vector $\hat{f}$. Let $\vec{N}$ be the vector describing the needle orientation having a magnitude N in the direction of the unit vector $\hat{n}$. The frequency perturbation is then $F^2N^2 (\hat{f}\cdot\hat{n})^2$.

Consider the right handed coordinate system where $\hat{z}$ coincides with the axis of needle rotation, $\hat{x}$ passes through the center of the needle normal to $\hat{z}$ in the horizontal plane, and $\hat{y} = \hat{z} \times \hat{x}$.
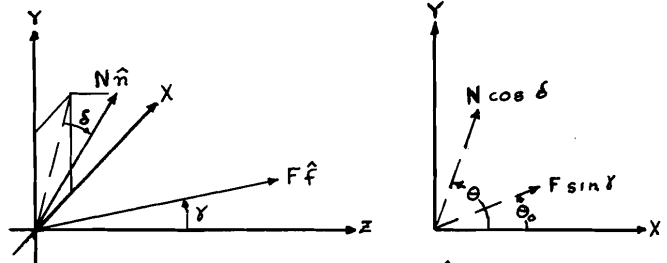
Let Y be the angle between $\hat{z}$ and $\hat{f}$, δ be the angle from the xy plane to $\hat{n}$ (the needle misalignment), θ_0 be the angle between $\hat{x}$ and the projection of $\hat{f}$ on the xy plane, and θ be the angle between $\hat{x}$ and the projection of $\hat{n}$ on the xy plane. The unit vectors can be written

$$\hat{f} = \sin Y \cos \theta_0 \hat{x} + \sin Y \sin \theta_0 \hat{y} + \cos Y \hat{z}$$

$$\hat{n} = \cos \delta \cos \theta \hat{x} + \cos \delta \sin \theta \hat{y} + \sin \delta \hat{z},$$

and the dot product becomes

$$(\hat{f}\cdot\hat{n}) = \sin Y \cos \delta \cos (\theta-\theta_0) + \cos Y \sin \delta$$

For small Y and δ, the dot product reduces to

$$(\hat{f}\cdot\hat{n}) = Y \cos (\theta-\theta_0) + \delta$$

and the frequency perturbation (dropping the constant factor F^2N^2) can be written

$$P(\theta) \cong \left(\frac{Y^2}{2} + \delta^2\right) + 2Y\delta \cos (\theta-\theta_0) + \frac{Y^2}{2} \cos 2(\theta-\theta_0).$$

(3)

The perturbation as a function of θ has a first harmonic term of amplitude $A_1 = 2Y\delta$, and a second harmonic term of amplitude $A_2 = Y^2/2$.

The angles Y and θ_0 contain the information on the fields that we wish to know. The angle Y is equal to $4\delta A_2/A_1$. By using needles of known misalignment (δ), and determining A_2/A_1 from the recorded frequency excursions, it is possible to evaluate Y.

Notice that $P(\theta)$ is symmetric about $\theta = \theta_0$ and $\theta = \theta_0+180°$. These points of symmetry are easily recognized on the data (see Fig. 8). Let the point of symmetry representing the largest perturbation (lowest resonant frequency) be the case where $\theta = \theta_0$. In order to establish a direction in space for θ_0, it is necessary to determine the spatial orientation of the needle θ at the moment when $\theta = \theta_0$. Data regarding the needle orientation was recorded automatically by superimposing a small electrical pulse on the input to the chart recorder when the "head" of the needle was up ($\theta = 90°$). It is now possible to interpolate

between these marks to determine θ at any point, and in particular, at the point $\theta = \theta_0$.

Transverse Field Data

The transverse needle measurement technique was used on our 35-cell model. The needle was mounted on a hollow 1/16-in. diam ceramic rod that extended through cells 33, 34, and 35 ending up outside the cavity as shown in Fig. 7. The rod was motor driven at a speed of 6 rpm. Data was taken with the needle in three different axial positions in gap 33 as shown in the figure. Two different needles were used, both of which had a length of 1 in. and a diameter of 0.014 in. The needles differed in their degree of misalignment, namely $\delta = 1°$ and $\delta = 4°$.

Three typical traces of the data obtained with this technique are shown in Fig. 8. The total frequency variation per period is about 120 Hz for the upper trace, 60 Hz for the center trace and 40 Hz for the lower trace. The general tilts on these traces are due to gradual drifts in the resonant frequency of the structure. The lines and numbers on the two lower two traces were constructed for the purpose of determining the ratio of the amplitude of the second harmonic to the amplitude of the first harmonic (A_2/A_1). The arrows on all three traces call attention to the electrical pulses introduced to reveal the needle orientation.

The top and center traces were taken under similar tank conditions, but on different days. In each case, the resonant frequency of end cell 1 was raised 7 MHz, the resonant frequency of end cell 35 was lowered 7 MHz, and the needle was centered on gap 33. The upper trace was produced by the $\delta = 4°$ needle and yields values of $\gamma = 4.0°$ and $\theta = 90°$. The center trace, which looks quite different, was produced by the $\delta = 1°$ needle and yields values of $\gamma = 6.0°$ and $\theta_0 = 90°$.

The lower trace was taken where the resonant frequency of cell 1 was 3.5 MHz high, the resonant frequency of end cell 35 was 3.5 MHz low, and the needle was located 1 in. from drift tube 33. The trace was produced by the $\delta = 1°$ needle and yields values of $\gamma = 2.4°$ and $\theta_0 = 118°$.

Figure 9 shows a collection of values for γ as a function of end cell perturbations. Some of the data was taken with the $\delta = 1°$ needle, and some of the data was taken with the $\delta = 4°$ needle. Although the frequency excursions produced by the two needles are quite different as indicated in Fig. 8, the values of γ determined by this technique are in good agreement.

Table 1 and Fig. 10 present the results of 9 transverse field measurements taken in gap 33 of the 35 cell model with post couplers. The 9 measurements correspond to 3 needle positions within the gap for each of 3 end cell tuning error configurations. The needle positions in gap 33 (gap length $\sim$ 4 in.) are

1) 1 in. from drift tube 32,
2) on center of gap 33,
3) 1 in. from drift tube 33.

The end cell tuning error configurations are

1) Cell 1 raised 7 MHz, cell 35 lowered 7 MHz,
2) Initial conditions (no errors),
3) Cell 1 lowered 7 MHz, cell 35 raised 7 MHz.

Table 1 presents the values of γ and θ_0 as determined for the 9 cases. Figure 10 shows a polar plot of (γ, θ_0) for each needle position. These plots suggest that the transverse field vector is made up of a vertical component that is uniform across the gap and a horizontal component that is odd about the center of the gap. The graphs also demonstrate that even for crude alignment (data points B) the transverse fields vanish. The small and constant transverse field indicated by data points B could easily be explained by a small misalignment between the accelerating field and the needle axis.

Table 2 and Fig. 11 present the results of 6 transverse field measurements taken in gap 33 of the 35-cell model without post couplers. These measurements correspond to 2 needle positions within the gap for each of 3 end cell tuning error configurations. The needle positions correspond to the last two of the previous paragraph, and the tuning error configurations are

1) Cell 1 raised 0.7 MHz, cell 35 lowered 0.7 MHz,
2) Initial conditions (no errors),
3) Cell 1 lowered 1.0 MHz, cell 35 raised 1.0 MHz.

Table 2 presents the values of γ and θ_0 as determined for the 6 cases. Figure 11 shows a polar plot of (γ, θ_0) for both needle positions. The tuning errors used to produce these fields are an order of magnitude smaller than in the case of the post coupled structure. It was not possible to use larger end cell perturbations in this case without post couplers, because the resulting field tilts were so large that the structure would not oscillate in the proper mode. Because of this narrow range of end cell perturbations and due to the uncertainties in the measurements, the direction and magnitude of the transverse fields are not as well determined here as they are in the case of the post coupled structure.

With this reservation in mind, it is still worth noting that Fig. 10 reveals a total change in transverse field $(\Delta\gamma)$ of 8° for a total change in end cell frequency of 14 MHz, whereas Fig. 11 reveals a total change in transverse field $(\Delta\gamma)$ of 1° for a total change in end cell frequency of 1.7 MHz. The ratio in both cases is 0.6°/MHz, so that it appears that the amount of transverse field arising from a given end cell perturbation is the same with or without post couplers.

Conclusions

Post coupler excitations have been shown to depend on tuning errors and power losses as predicted by the coupled resonator analysis. It was necessary to resort to very large tuning errors in order to produce measurable transverse fields on the axis of the linac. Tuning errors in an actual linac will certainly be 100 to 1000 times smaller than the tuning errors used here. The largest

transverse field measured here $(\gamma = 6°)$, when reduced by a factor of 100, would produce a transverse impulse that is very small compared to the radial impulse received by the average particle on crossing the gap. The quadrupole focusing system can easily counteract transverse fields of these magnitudes.

Acknowledgments

References

1. D. E. Nagle, E. A. Knapp, and B. C. Knapp, "Coupled Resonator Model for Standing Wave Accelerator Tanks," RSI $\underline{38}$, 11, p. 1583 (1967).

2. E. A. Knapp, J. M. Potter, E. J. Schneider, and D. A. Swenson, "Stabilization of the Drift Tube Linac by Operation in the $\pi/2$ Cavity Mode," (MP-3/EAK/JMP/EJS/DAS-1), June 2, 1967, unpublished.

3. D. A. Swenson, E. A. Knapp, J. M. Potter, E. J. Schneider, "Stabilization of the Drift Tube Linac by Operation in the $\pi/2$ Cavity Mode," Sixth International Conf. on High Energy Accelerators, Cambridge, Mass., CEAL-2000.

4. G. R. Swain, "Analysis of Multiply-Coupled Resonators Using a Matrix Formulation," (MP-3/GRS-7), unpublished.

5. G. R. Swain, "Sensitivity to Tuning Errors for a Multiply Coupled Biperiodic Chain of Resonators Terminated in Full Cells," (MP-3-8), un published.

6. E. A. Knapp, B. C. Knapp, and J. M. Potter, "Standing Wave High Energy Linear Accelerator Structures," to be published in RSI, June 1968.

Tuning Errors (MHz)		Needle 1" From Drift Tube 32		Needle Centered on Gap 33		Needle 1" From Drift Tube 33	
Cell 1	Cell 35	γ	θ_o	γ	θ_o	γ	θ_o
+7.0	-7.0	2.8°	73°	6°	90°	3.5°	124°
0	0	0.8°	90°	1°	90°	1.0°	90°
-7.0	+7.0	1.8°	263°	2°	270°	2.3°	310°

Table 1   Transverse Field Data (with post couplers)

Tuning Errors (MHz)		Needle 1" From Drift Tube 32		Needle Centered on Gap 33		Needle 1" From Drift Tube 33	
Cell 1	Cell 35	γ	θ_o	γ	θ_o	γ	θ_o
+0.7	-0.7			1.3°	37°	1.2°	53°
0	0	NO DATA		1.6°	33°	1.6°	46°
-1.0	+1.0			2.0°	15°	2.0°	29°

Table 2   Transverse Field Data (without post couplers)

Fig.1. Post Coupled Drift Tube Linac Structure
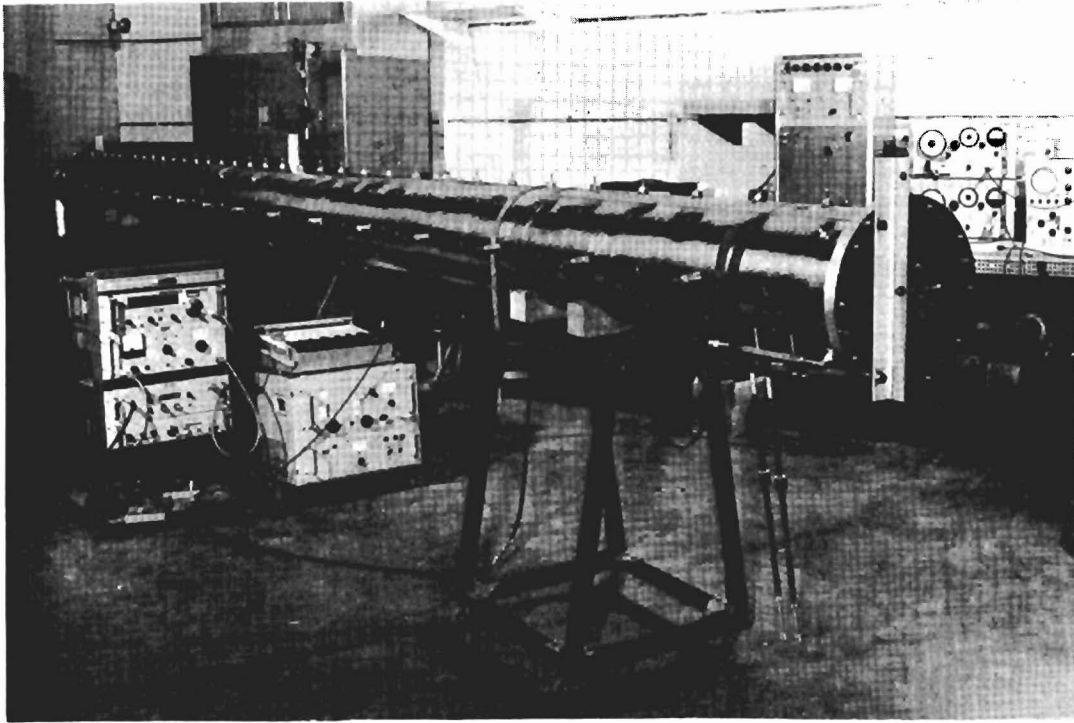
Fig.2. 35-Cell Post Coupled Drift Tube Linac Model
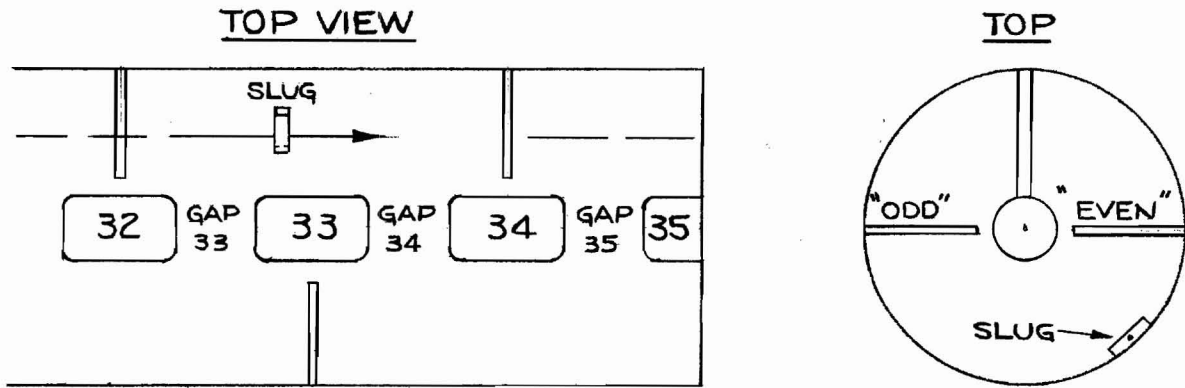
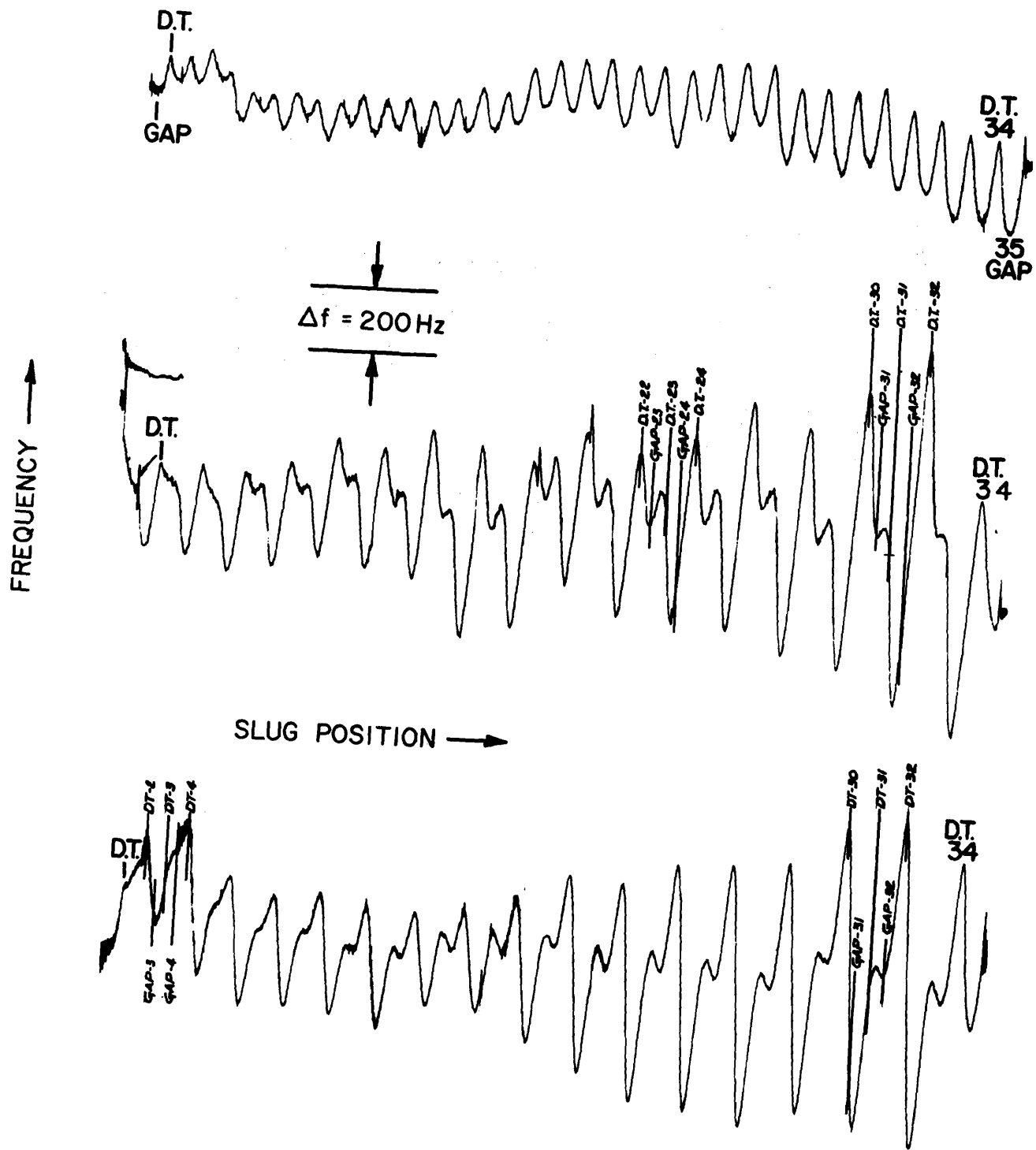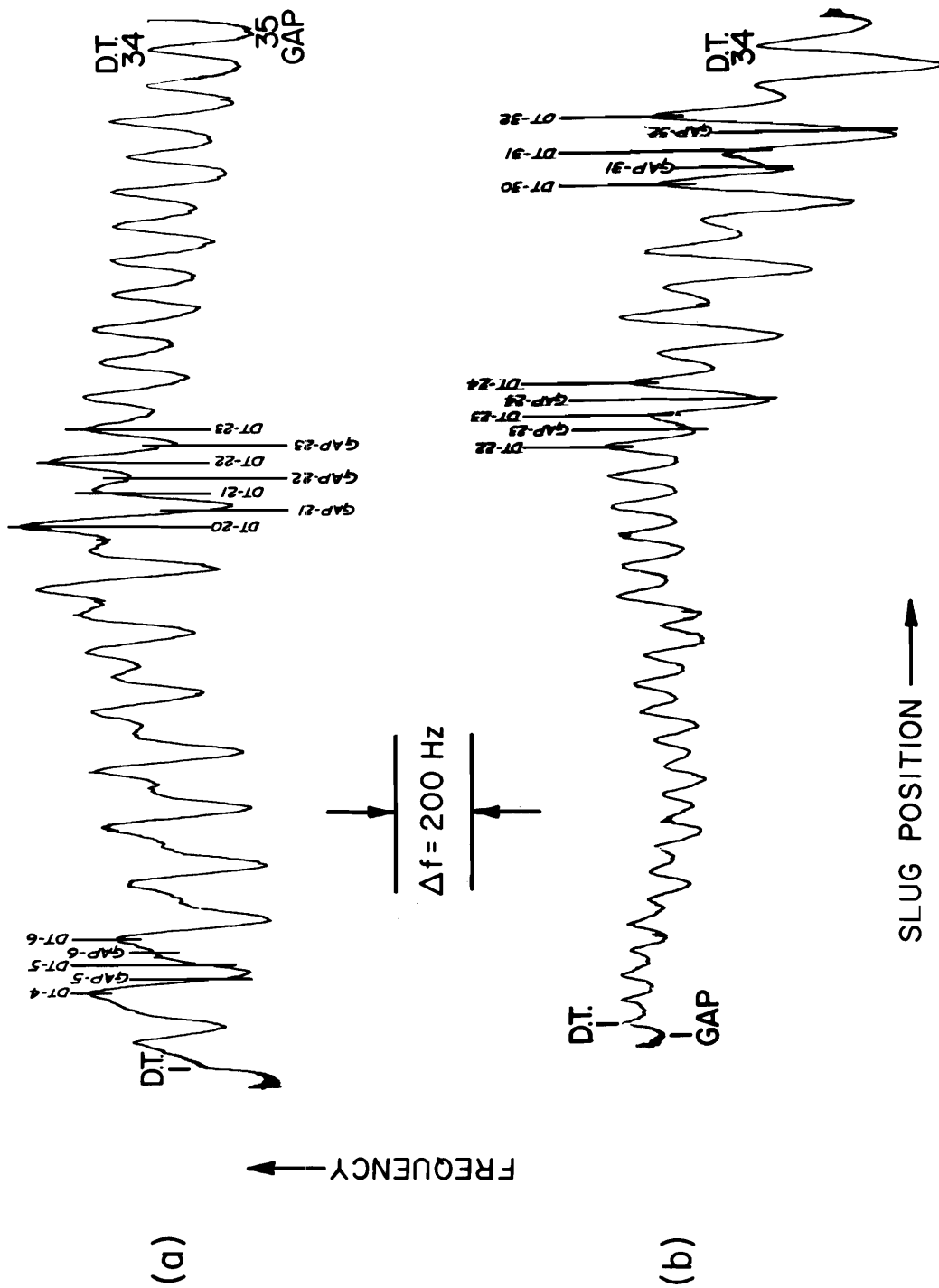Fig.3. Experimental Setup for Measurement of Relative Post Excitations

FREQUENCY →

D.T.
GAP

Δf = 200 Hz

D.T.

DT-22
GAP-23
DT-23
GAP-24
DT-24

DT-30
GAP-31
DT-31
GAP-32
DT-32

D.T.
34

D.T.
34

35
GAP

SLUG POSITION →

D.T.
1

DT-2
GAP-3
DT-3
GAP-4
DT-4

DT-30
GAP-31
DT-31
GAP-32
DT-32

D.T.
34

Fig.4.   Post Coupler Excitation Data

Fig.5. Post Coupler Excitation Data
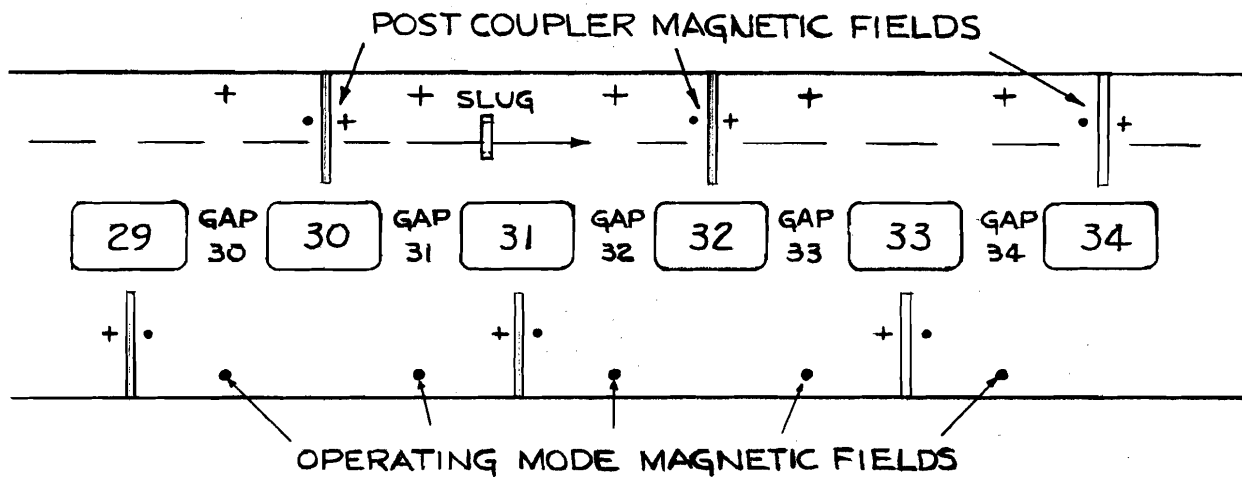
Fig.6. Superposition of Magnetic Fields of Operating Mode and Post Couplers
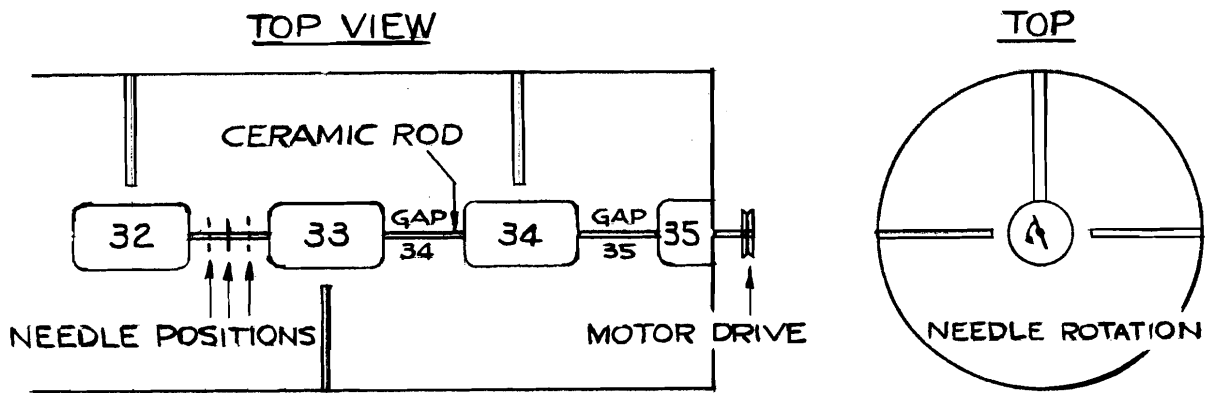
Fig.7. Experimental Setup for Measurement of Transverse Fields
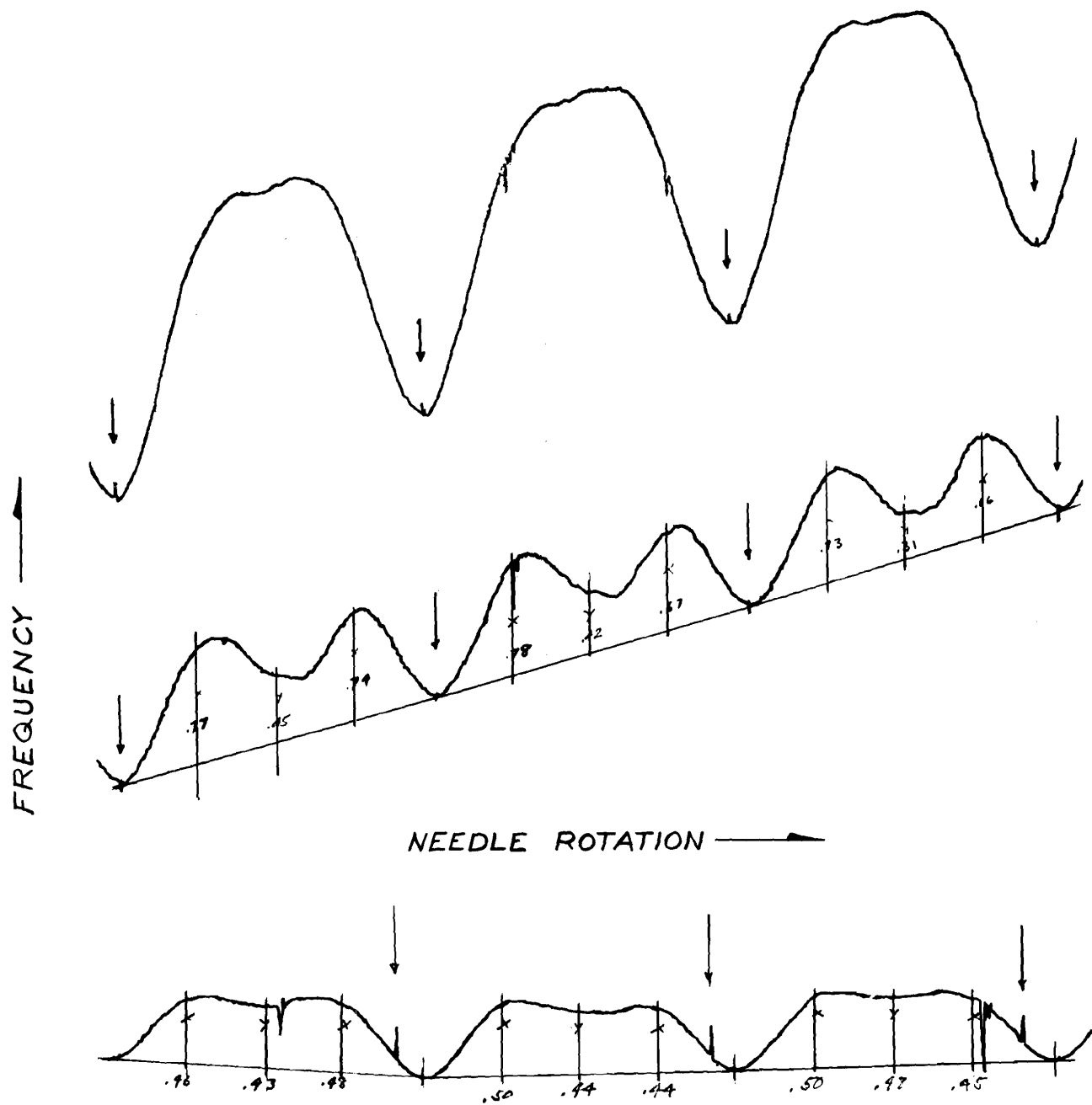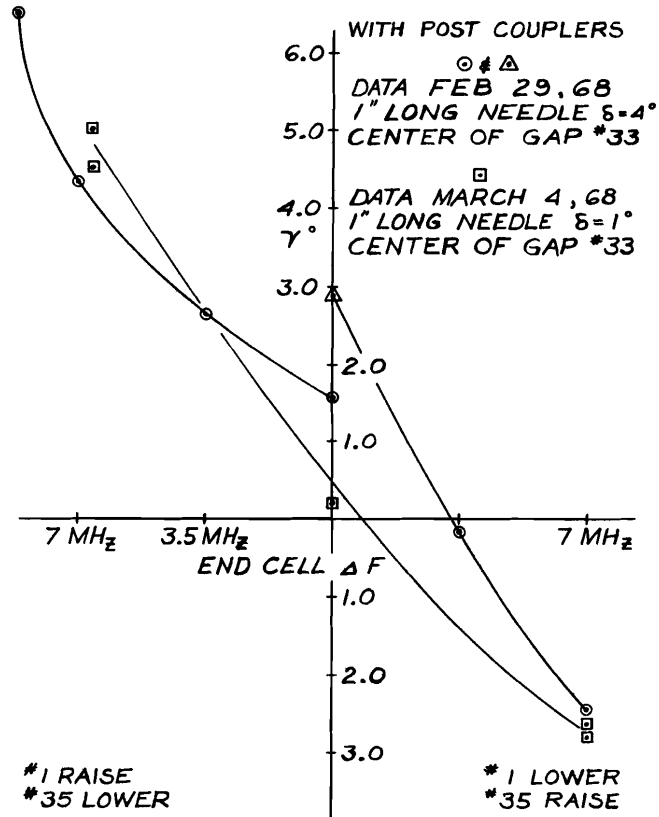
Fig.8. Transverse Field Data

Fig.9.   Comparison of Transverse Field Data Taken with Needles of
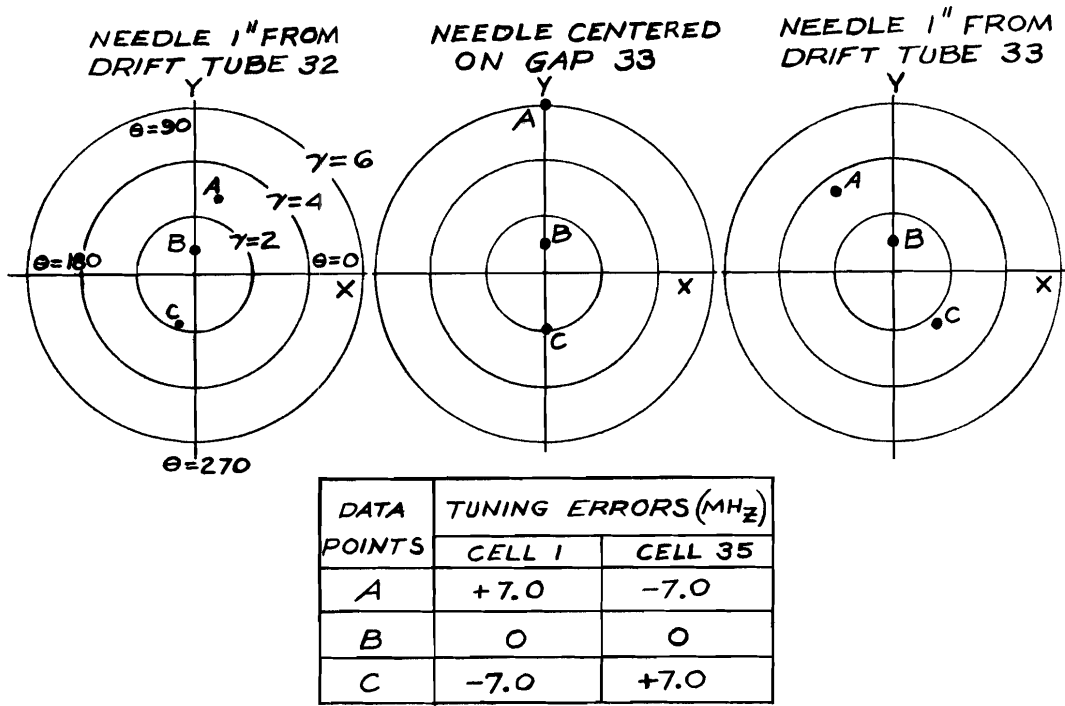   Different Misalignments

Fig.10. Polar Plot of Transverse Field Data for Structure with Post Couplers
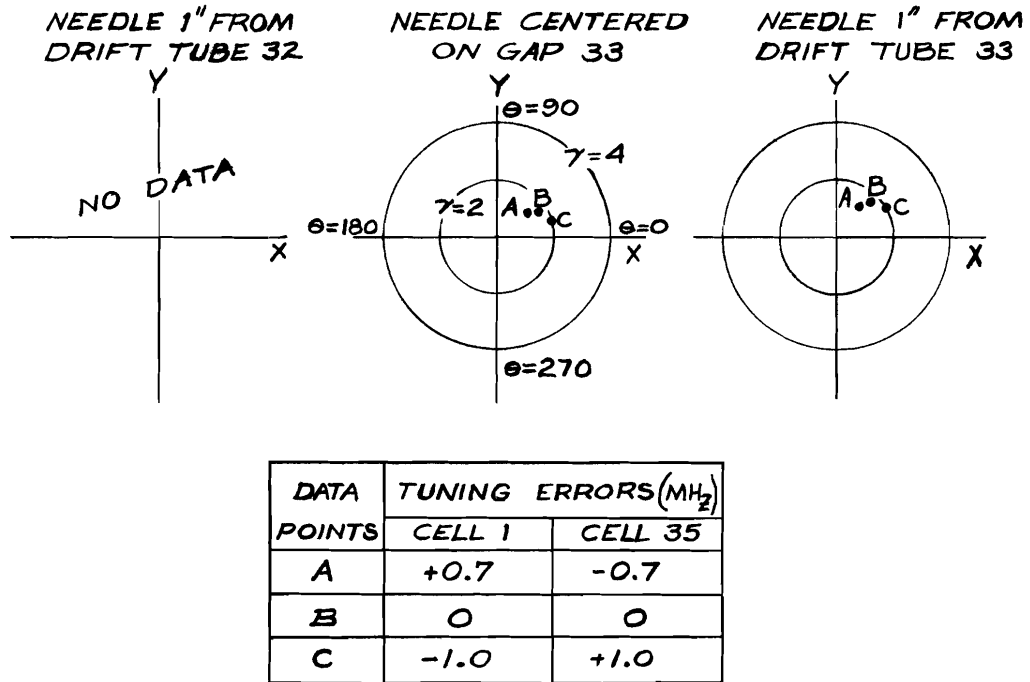

Fig.11. Polar Plot of Transverse Field Data for Structure without Post Couplers